Magnetic lightning in macroscopic superconducting ring structures

Alejandro V. Silhanek[0000−0001−9551−5717]

Abstract In this chapter, we discuss the process of magnetic flux injection into a macroscopic flat superconducting ring. We place special emphasis on the emergence of lightning-like magnetic flux bursts along heated trails originating from thermomagnetic instabilities. Additionally, we explore strategies aimed at mitigating or delaying this phenomenon. Understanding these dynamics is crucial, as they may significantly impact the performance of superconducting resonators, shielding systems, and metamaterials.

1 Introduction

The physics of multiply-connected superconducting structures, especially superconducting rings, has sparked genuine academic interest since early times. Bibliographic research shows about 5000 scientific publications in the last 50 years [1]. This fascination arises in part from the constraint imposed by the fluxoid quantization and the fact that the ring defines two regions of the universe separated by a physical gap within which the magnetic flux remains excluded. The year 1967 seems to set a particular moment in the story of superconducting rings with the appearance of two seminal scientific contributions [1, 2]. At the time, scientists recognized that a persistent current running in a one-dimensional ring represents a metastable state with high kinetic energy, whereas the ground state corresponds to the state with no supercurrents. Then, the question about the lifetime of this metastable state in ring-shaped specimens was addressed and understood based on topological fluctuations (both in phase and amplitude), which lead to a state of lower current and, therefore, lower free energy [1, 2]. These fluctuations on 1D rings correspond to a depletion of the order parameter down to zero value, thus permitting the phase to jump by arbi-

Alejandro V. Silhanek
Université de Liège, Allée du 6 août 19, Sart Tilman, B-4000 Liège e-mail: asilhanek@uliege.be

[1] Scopus document search for “superconducting ring” as title, abstract, or keyword.

trary multiples of $\pm 2\pi$. They can be of thermal origin, so-called thermal phase slips [3, 4, 5, 6, 7, 8], or arising from quantum tunnelling of the phase, known as quantum phase slips [9, 10, 11, 12]. This is a rather universal behaviour in which the material aspects are of secondary importance, besides the fact that the spatial extension of the fluctuations (i.e. the size of the created normal region) scales with the coherence length $\xi(T)$, if the wire has a diameter $d < \xi(T)$. Whether the superconductor is of type I or type II makes no difference.

Phase slips also appear in 1D superconducting rings under increasing external magnetic field, H. At low applied fields, the magnetic flux is screened from the interior of the ring until a certain field, H_p, at which a phase-slip event will permit the injection of magnetic flux inside the ring in such a way to guarantee fluxoid quantization [3, 4, 5, 6, 7, 8]. At temperatures, T, close to the critical temperature, T_c, this effect leads to Little-Parks periodic oscillations [13, 14] as a function of H exhibiting resistance minima when the flux piercing the ring equals $(2n + 1)\Phi_0/2$, with n an integer and $\Phi_0 = h/2e$ the quantum of magnetic flux. These oscillations are imprinted in the typical parabolic phase boundary caused by the suppression of superconductivity with magnetic field [15] and can be accounted for within the Ginzburg-Landau theory [14]. At lower temperatures, when $T \ll T_c$, oscillations are also reflected in the critical current of the ring with a response which becomes similar to a SQUID (superconducting quantum interference device) [16, 17], albeit with a marked irreversibility. A transition from one regime to another has been reported in Ref.[18]. It is worth mentioning that an intermediate and stable phase in which the ring is interrupted by a normal state region has been predicted in Ref.[19, 20].

If we move away from the 1D condition to consider rings with wide and long walls thus approaching a cylindrical structure, a different phenomenology should be taken into account. For a ring of outer and inner radii R_o and R_i, respectively, the width of the ring is $w = R_o - R_i$. Likharev [21] has shown that vortices can nucleate in thin walls only if $w \geq 4.44\xi(T)$. In this limit, the formation of phase-slips evolves into phase-slips-lines, which can be regarded as a passage of a vortex crossing the width of the ring [22]. Trapped vortices in the width of the ring could also account for the observed parabolic background envelope of the Little-Parks oscillations [23]. For larger w (i.e. larger than the penetration depth λ) the possibility of vortex-antivortex nucleation and annihilation should be considered. Eventually, for superconducting rings with very wide walls in which pinning centers are present, the critical state model, describing inhomogeneous distribution of vortices, should be taken into account [24].

In the scope of this study, we will not be considering mesoscopic structures for which $w \sim \xi$. This limit has been thoroughly examined in Ref.[25, 26, 27, 28, 29, 30] for single rings and more exotic structures such as Möbius loop [31, 32] and gradiometer configuration (eight-shaped loop) [33]. Instead, our attention will be directed into macroscopic rings with $w \gg \xi$ which have the capacity to accommodate a large amount of vortices.

2 Long cylinder in axial configuration

It is instructive to start this journey by reviewing the physics of long and thick cylindrical cavities with an axially applied magnetic field, for which the demagnetization effects can be neglected (see Fig.1(a)). Note that in zero-field cooling (ZFC), as long as the applied magnetic field remains below a certain penetration field H_p, there are supercurrents circulating only on the outer surface. For $H > H_p$, however, counter currents develop in the inner surface. In the early 60's, Kim et al.[34] experimentally investigated how the transition from field shielding to flux filling occurs. Fig.1(b) shows the magnetic field H' picked up inside a tubular NbSn sample as a function of the externally applied field H. The magnetic field remains screened out from the interior of the cylinder until H reaches H_p ($H \sim 15$ kOe, labelled (1) in Fig.1(b)). At that point, part or the entire tube suddenly becomes normal and the flux breaks into the interior of the tube through a flux jump [35] (also known as flux avalanche). After such a flux jump occurs, H is held constant for several minutes to allow the sample to reach thermal equilibrium with its surroundings. As H is further increased, the tube again shields the external field until it undergoes another flux jump at point (2). Note that at point (3), the transition becomes smoother, which is interpreted as an indication that the critical state front starts pouring vortices inside the tube.

It has been demonstrated that a superconducting cylinder in longitudinal geometry and for $H < H_p$ can act as an excellent passive screen against magnetic fields over a large frequency range and performs better than a ferromagnet at low frequency [36]. Fig.1(c) shows that if the cylinder is not infinitely long, the shielding factor H/H' is not infinite since H' cannot be zeroed. Indeed, some of the field lines penetrate through the top and bottom openings and, for small fields, decay exponentially with distance as moving away from the center of the cylinder. The field lines depicted in Fig.1(d) show an interesting feature: the magnetic field lines change direction along the upper and lower rims, both exhibiting a component opposite to the applied field. It may then be expected that a negative field at the inner rim develops as the cylinder becomes progressively shorter (flatter) when approaching a ring structure.

3 Superconducting flat ring in the Meissner state

In the thin film geometry, there are some particularities which stand out with respect to long cylinders [24, 37]. For a positive applied field and $H \ll H_p$,[2] i.e. long before vortices can reach the inner edge of the ring, the local field at the inner rim of the ring is negative and turns positive at the center of the ring. This has been experimentally demonstrated by direct visualization of the field distribution via magneto-optical image, as shown in Fig.2(a) for a 100 nm-thick $YBa_2Cu_3O_7$ ring ($R_o = 3$ mm, $R_i = 2.875$ mm) at $T = 4.2$ K [37]. Panel (b) shows a sketch of the magnetic field

[2] Warning note: The definition of H_p in Ref.[24, 37] does not concern vortex penetration but rather the onset of saturation magnetization.

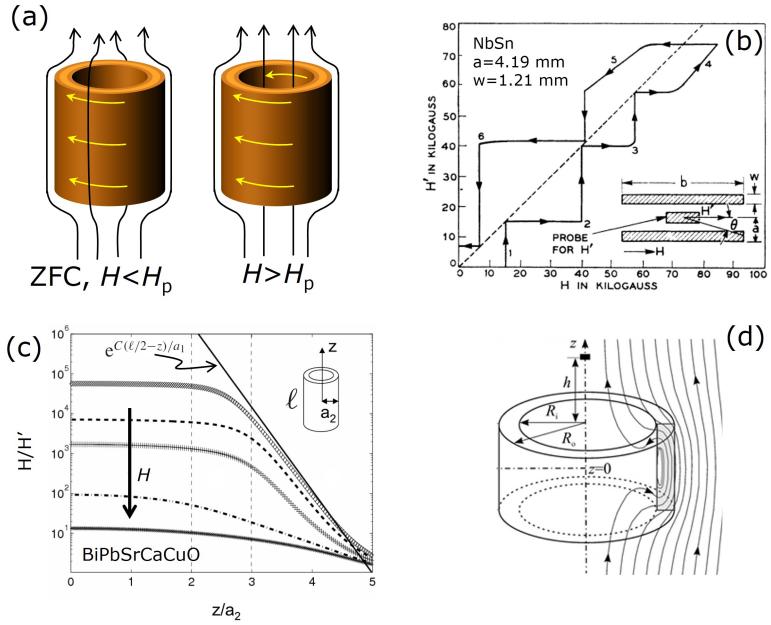

Fig. 1 (a) Superconducting cylinder under an applied field along the axial direction. When the field has been applied after cooling in zero field (ZFC) and remains below the penetration field H_p, screening currents circulate on the outer surface (left panel). For $H > H_p$ the field is able to penetrate into the cylinder and currents of opposite chirality circulate in the inner and outer surface of the cylinder (right panel). (b) The transition between the two states described in panel (a) can be abrupt as indicated by the step-wise increase 1 and 2 due to flux jumps, or smooth (as in 3 and 4), caused by the progressive penetration of superconducting vortices. The inset shows details related to the ring geometry. Reprinted figure with permission from [34]. Copyright 1963 by the American Physical Society. (c) The screening factor of the cylinder depends on the position along its axis, being rather constant at its center if $\ell > 6R_o$. The leakage of magnetic flux lines at the top and bottom ends of the cylinder gives rise to an exponential decay of the screening factor. (d) The region of constant shielding factor disappears for short cylinders $\ell < 6R_o$. Note that the magnetic stray field at the extremities has a component opposite to the applied field. Figure reproduced from [36].

lines, whereas the non-uniform distribution of currents for several applied fields is shown in panel (c). The magnetic field profiles as H increases are shown in panel (d), in which the strength of the peaks at the inner and outer borders of the ring scales with the width/thickness ratio. These authors also show that after exceeding H_p and during the field reversal, a situation arises in which currents of similar polarity can circulate along the inner and outer rims, whereas at the center of the ring a counterflow current is maintained. Thus, three concentric current loops with antiparallel flow may coexist.

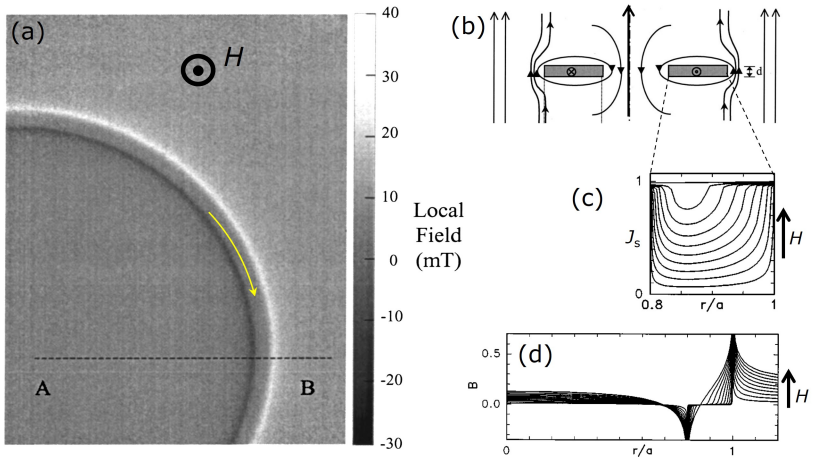

Fig. 2 Magneto-optical image of a section of a 125 μm wide YBCO ring at 4.2 K and after zero-field cooling $\mu_0 H = 8$ mT. (b) Sketch showing the magnetic field lines generated by the supercurrent flowing in the ring superposed to the applied magnetic field. Reprinted figure with permission from [37]. Copyright 2001 by the American Physical Society. Profiles of the sheet current J_s (c) and perpendicular magnetic field B (d) as a function of the radial coordinate r in a ring with $R_o = a$ and $R_i = 0.8R_o$ for several increasing applied fields H, according to the Bean model. Reprinted figure with permission from [24]. Copyright 1997 by the American Physical Society.

4 The perforation field

The progressive filling in of the ring's core with magnetic flux has been experimentally addressed by Nowak et al.[38]. The system under investigation consisted of a 500-nm-thick Nb ring with $R_i = 15$ μm and $R_o = 98$ μm in which two Bi Hall probes able to measure the out-of-plane component of the local field in an area of 3 μm × 5 μm, are placed at the center of the ring (hole probe) and 22 μm off center (ring probe) as schematically shown in the inset of Fig.3(a). Note that the investigated system is substantially smaller (about 40 times) than the one previously investigated by Kim et al. [34]. The main findings of this report are shown in Fig.3(a-c). Panels (a,b) show the hysteresis loops, $B(H)$, at two reduced temperatures, $t = T/T_c$, for the ring probe (thin line) and the hole probe (thick line). Smooth vortex motion at high t [panel (a)] is replaced by avalanche behavior at lower temperature [panel (b)]. The inset of panel (b) sketches the magnetic field profile in a cross-sectional view of the ring. Solid lines (dashed lines) represent the profile immediately before (after) an avalanche. By quantifying the size of the jumps[3] along a hysteresis loop as the one shown in panel (b), it is possible to identify two distinct regimes of magnetic flux avalanches. Indeed, panel (c) shows the size of the avalanches detected by the hole probe as a function of the reduced temperature in which a regime of small-size

[3] The size of the avalanches in units of the flux quantum, as detected by the hole probe, is obtained by multiplying the field jump by the area of the inner hole.

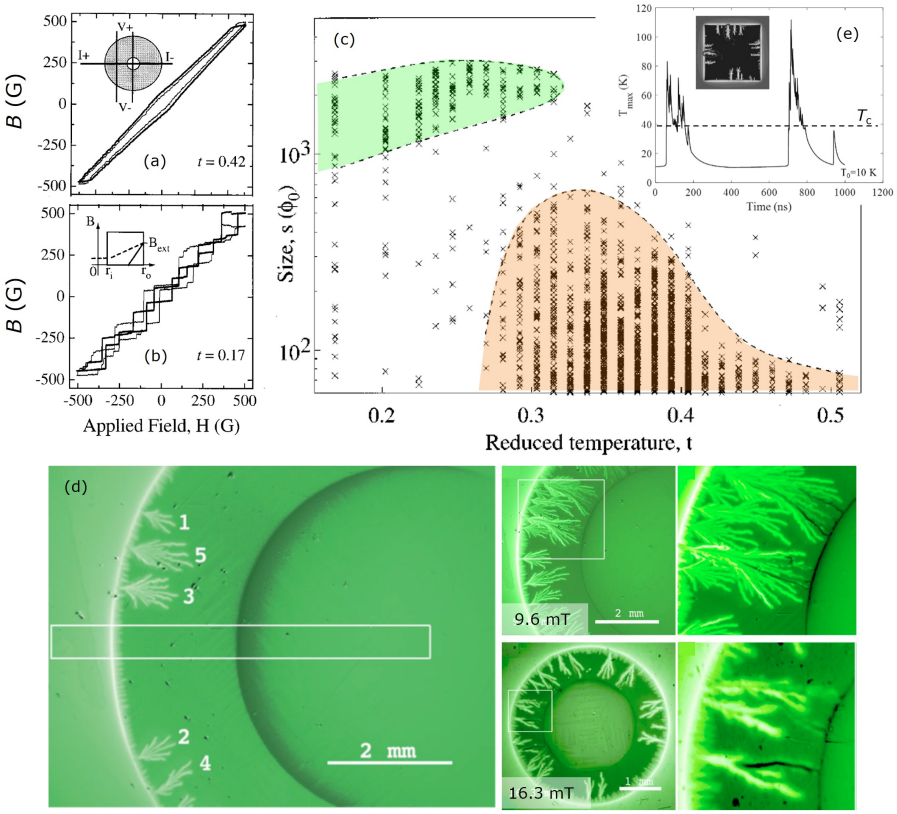

Fig. 3 Hysteresis loops, $B(H)$ obtained while ramping the external magnetic field at $t = T/T_c = 0.42$ (a), and $t = 0.17$ (b) for a Hall probe positioned in the ring width (thin line) and a Hall probe parked at the center of the inner hole (thick line). Dynamically driven vortex avalanches lead to a smooth response at high temperatures and thermally driven avalanches manifest themselves as jumps in the local field. The inset of (a) shows the sample's ring geometry and the positions of the Hall probes. The inset of (b) sketches the magnetic field profile in a cross-sectional view of the ring with solid lines (dashed lines) representing the profile immediately before (after) an avalanche. (c) Scatter plot of the observed avalanches as detected by the Hall probe inside the hole of the ring as indicated in panels (a,b) as a function of $t = T/T_c$. The colored regions are a guide to the eye indicating the regions of thermomagnetically driven avalanches (green) and small-size dynamically driven avalanches (orange). Reprinted figure with permission from [38]. Copyright 1997 by the American Physical Society. (d) (left panel) Magnetic flux distribution in a MgB_2 ring at 3.6 mT. The numbers next to dendrites indicate the order in which they appeared. (middle column) magneto-optical images after zero-field-cooling a large ring (upper panel) and a small ring (lower panel). In both images the antidendrites nucleate near a bright tip, in most cases tracing a bright finger deep into the superconductor. The areas within the rectangles are shown in more detail in the right column. Reprinted figure with permission from [40]. Copyright 2006 by the American Physical Society. (e) Simulated local temperature rise during magnetic flux avalanche process for a superconducting sample with $T_c = 39$ K (courtesy from Prof. Cun Xue).

avalanches (dynamically driven or isothermal avalanches) is visible at high temperatures ($t > 0.27$), whereas large size avalanches (thermally driven or adiabatic) develop at low temperatures ($t < 0.32$) [39]. In summary, the center of the ring can be filled in with magnetic flux either smoothly and progressively via injection of small bundles of vortices or via an abrupt burst of big avalanches able to inject large amount of vortices (somewhat similar to the conclusion of Ref.[34]). Note that there exists an intermediate temperature range in which these two regimes coexist, in agreement with the results presented in Ref. [39]. Eventually, as t increases, the size of avalanches decreases, and the phenomenon disappears, leading to a nearly continuous $B(H)$ curve.

Unfortunately, the Hall sensors used in Ref.[38] are unable to reveal the details of the process of flux injection. In order to fill this gap, large-scale imaging is needed, which is precisely what has been done by Olsen et al.[40] who visualized via magneto-optical imaging the flux injection due to magnetic flux avalanches in a MgB_2 ring. The rings analyzed in this work were substantially larger than those of Nowak et al.[38], with R_o, R_i, and $R_o - R_i$ on the mm scale. The large demagnetization field of these structures when the field is applied along the axial direction gives rise to pronounced magnetic field peaks of opposite polarity at the outer and inner edges (as those described in Fig.2), which in turn favors the penetration of vortices from the outer edge and antivortices from the inner edge. At low temperatures, branching dendritic magnetic avalanches [41, 42] nucleate at the outer edge and abruptly propagate deep into the rings, although without crossing the entire width of the ring. When these structures reach close to the inner edge, where flux with opposite polarity has penetrated the superconductor, they occasionally trigger anti-flux-dendrites. These antidendrites do not branch, but instead trace the triggering dendrite in the backward direction (see Fig.3(d)).

Magnetic lightning

One cannot avoid noticing the similarity of the phenomenon described above with a lightning strike [43] in which negative flashes (could also be positive) bring negative (or positive) charge to the ground. In negative flashes, the descending current from the cloud moves downward in a series of short jumps, called a "stepped leader." The individual steps in this process branch out in different directions, looking for the path of least resistance toward the ground. As a leader gets close to the ground, a corresponding streamer of positive charge moves up from the surface to meet the descending negative current. When these two currents connect, they provide a highly conductive channel for charge transfer between the cloud and the ground. The initial descending negative charge is followed by an even stronger "return stroke" of positive charge from the ground, which seems to move up, retracing the channel and into the cloud [44]. While lightning corresponds to a discharge of electric charges permitting the relaxation of an out-of-equilibrium state, flux avalanches in a superconductor correspond to magnetic lightning releasing magnetic pressure

difference. In other words, the dielectric breakdown phenomenon becomes a thermomagnetic breakdown in the case of superconductors.

The authors of Ref.[40] pointed out that by increasing the applied field further, the rings are perforated by dendrites, which carry flux to the central hole. This direct flux injection has been coined *magnetic perforation*. Repeated perforations lead to an increase of the average flux density at the inner edge to positive values (i.e. reversed field polarity with respect to the Meissner phase) thus reversing the current direction at the inner edge and impeding the nucleation of antiavalanches. It has been estimated experimentally and numerically [43, 45, 46], that flux avalanches propagate at speeds $\sim 10 - 100$ km/s which implies a growth time of $\sim 10 - 100$ ns, whereas the local temperature along the trail increases [43, 47, 48] to about $2.5T_c$ (see Fig.3(e)). This indicates that the propagation front consists of a normal-superconductor interface rather than a river of vortices, thus questioning the terminology "vortex avalanches". In any case, the precursor phase is certainly linked to the fast displacement of vortices in the material and the subsequent formation of kinematic vortices [49, 50, 51, 52].

Before closing this section, we would like to remind the readers the results of Ref.[53] on superconducting strips, in which the authors demonstrated that avalanche activity and size are progressively suppressed as the width of the superconductor decreases and are fully absent below certain threshold value. This result holds if the magnetic field penetrates from both sides of the strip. In this case, current circulates in opposite directions on opposite sides, which means that avalanches do not cross the symmetry line along the length of the stripe. The situation is different in a ring in the Meissner state, for which magnetic flux enters only through one side and screening currents circulate in a unique direction. This leads us to conclude that the width of the ring does not preclude the formation of flux avalanches.

5 Quasiperiodic injection

Further details of the abrupt magnetic injection (magnetic perforation) and the subsequent stages of flux pumping into the hole when increasing the applied magnetic field, were presented in Ref.[45]. The most salient results are summarized in Fig.4(a-c) for mm-scale flat rings of MgB_2. In panel (a), a field map of the sample at $T = 6.2$ K and $H = 13$ mT is shown (image I_n). Bright pixels correspond to positive magnetic field (out of the page), whereas dark pixels correspond to negative field. Note that avalanches are not able to perforate the ring. In this case, the supercurrents flow as indicated by the yellow arrows, everywhere in the same direction (clockwise). Panel (b) corresponds to the differential image $I_{n+1} - I_n$ in which at the (increasing) field step $n + 1$ an avalanche has perforated the ring injecting a large amount of flux in the center. While the most prominent feature is the large flux increase in the central hole, one can also observe a reduction in the field around the outer edge. After perforation,

the supercurrents along the inner edge reverse direction, as indicated by the yellow arrows in panel (b).

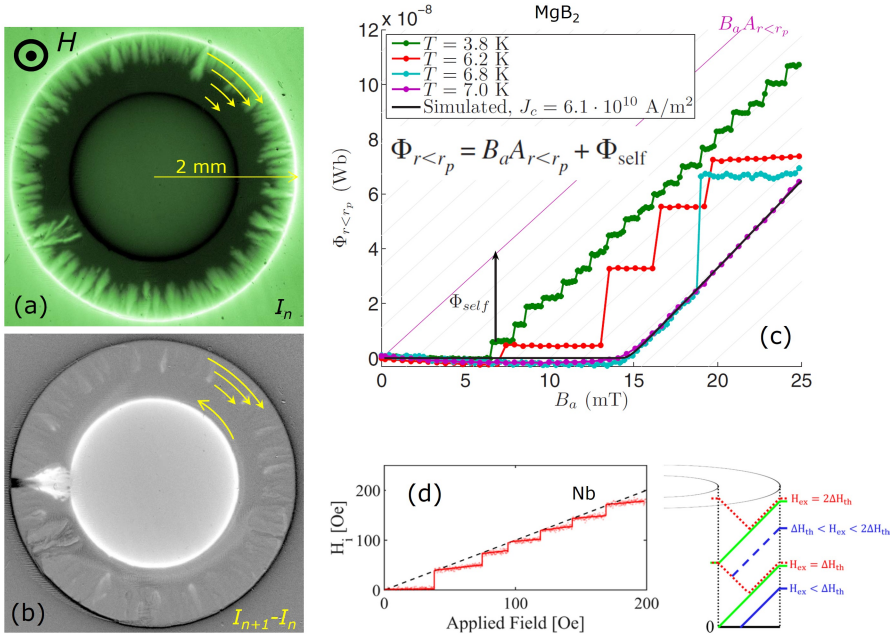

Fig. 4 (a) Magnetic field map of a MgB_2 ring at T = 6.2 K and 13 mT. Bright pixels correspond to positive magnetic field, while dark pixels correspond to negative fields. (b) Differential image between the image in panel (a) and the subsequent image after a dendrite has perforated the ring and injected a large amount of flux into the central hole. Bright and dark pixels indicate flux has entered or left. While the most conspicuous feature is the large flux increase in the central hole, one can also observe a reduction in the field around the outer edge. The arrows superimposed on the magnetic field maps show the current distributions before (a) and after the perforation (b). (c) Measured flux within a disk of radius r_p as a function of the applied field, showing the crossover from complete screening to a linear increase following the applied field. The flux jumps are small and frequent at low temperatures, becoming rarer and larger at higher temperatures. The contribution to the flux from the ring currents Φ_{self} is illustrated for one of the curves. The solid black line is the result of a simulation with a Kim model for the critical current. Reprinted figure with permission from [45]. Copyright 2007 by the American Physical Society. (d) The average field in the central hole of a small Nb ring as a function of the external field at 5 K. The solid red line is a guide to the eye. The stepwise increase in the field occurs when a dendrite crosses the entire rim of the ring. The dashed line corresponds to $H_i = H$. The sketch illustrates the mechanism for quasi-periodic jumps using a simplistic view for the case of a long cylinder. The green solid lines and the red dotted lines describe the magnetic induction just before and immediately after the appearance of a crossing dendrite, respectively. Reprinted figure with permission from [54]. Copyright 2019 by the American Physical Society.

The magnetic flux injected in a region delimited by the radius r_p (defined by the position at which the flux fronts from inner and outer edges meet at full penetration)

as a function of the applied field and for several temperatures, is shown in Fig.4(c). This radius r_p bears certain similarity to the effective radius limiting the area in which the flux is quantized in a mesoscopic ring, which is field-dependent and bounded by the inner and outer radii of the ring [29]. This similarity is to be expected, because in both cases r_p defines the condition of zero current density.

Provided that no perforation has occurred and the applied field is below the field of full penetration, this flux is zero (not so the magnetic field, as shown in Fig.2). At high temperatures (e.g. 7 K), the Meissner region ($\Phi = 0$) is followed by a linear increase in field starting at the penetration field. This regime is well explained by the conventional critical state model. The slope of the linear increase is the same as the one corresponding to an uniform field, since the currents have reached their saturation value everywhere and the screening remains constant. A different story unfolds at low temperatures, where avalanches appear and a step-wise (quasi-periodic) behavior is observed, with each step corresponding to an avalanche. The fact that the screening in the avalanche regime (quantified by Φ_{self}) is poorer than in the critical state indicates that the avalanches reduce the average screening current flowing in the ring. It is worth noting that the injection of flux is not enough to equal the external field with the internal one; there remains always a screening effect. As discussed below, this is not always the case, particularly in narrow rings.

Indeed, smaller Nb rings ($R_o = 800$ µm, and $R_o - R_i = 50, 100, 200, 300$ µm) investigated by Shvartzberg et al.[54] show that dendrites crossing the entire width of the ring appear when the difference between the applied field and the average field inside the central hole reaches a certain threshold level ΔH_{th} (see Fig.4(d)). This gives rise to a quasiperiodic step-wise increase of the inner field H_i. The authors show that ΔH_{th} increases with increasing $R_o - R_i$ whereas the first perforation field remains independent of $R_o - R_i$. Unlike the situation reported for large rings, in that work it is shown that the first nucleating dendrite always crosses the entire width of the ring. In addition, each injection of flux levels up the inner field with the applied field. Interestingly, in Ref.[55] it was theoretically predicted that the presence of pinning should lead to smaller steps in the staircase dependence.

Rigorous numerical modeling of the effects described above and including pinning (a weak quenched disorder is introduced by randomly decreasing the critical current density by 10% at 5% of the grid points) have been able to faithfully reproduce the experimental findings [46]. Fig.5 shows the numerical results for the case of MgB_2 with $T_c = 39$ K, i.e. corresponding to the experimental conditions of Ref.[40, 45]. At low temperatures, avalanches are triggered without leading to perforation, whereas at high temperatures, the first avalanche leads to perforation. After the applied field reaches about 11 mT at 20 K, the average magnetic field in the central hole increases linearly with the applied field due to the saturation of the current in the superconducting ring. Note that at high temperatures, the average field in the hole jumps to the value of the applied field. In contrast to that, at relatively low temperatures (7 K), the average field in the hole no longer jumps to the value of the applied field due to the shrinking of the heated flux channel with decreasing temperature, resulting in less flux being injected into the central hole. The threshold field H_{th} to trigger avalanches in a ring-shaped superconductor of constant outer

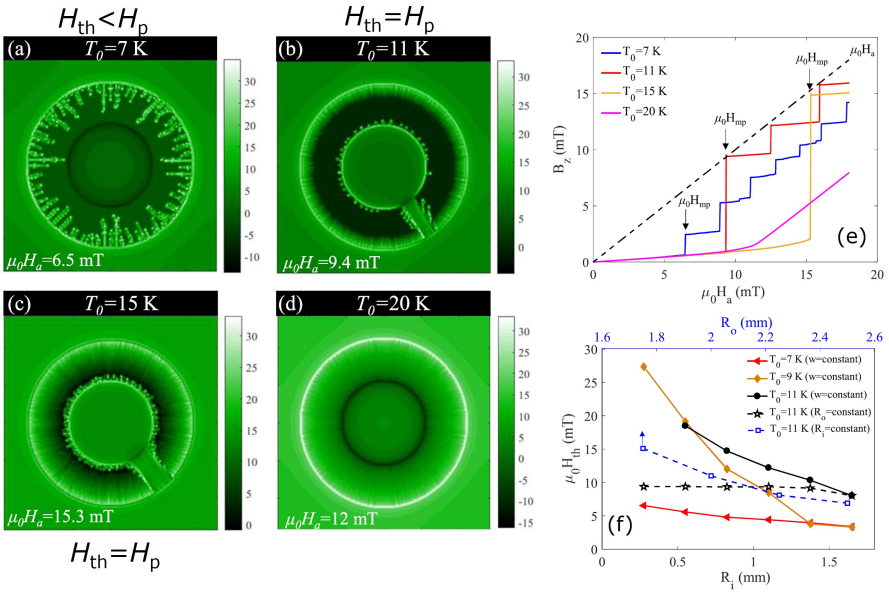

Fig. 5 (a-d) Simulated distributions of out-of-plane magnetic field in a single superconducting ring exposed to an increasing applied magnetic field with ramp rate 100 T/s at (a) T_0 = 7 K (magnetic perforation happens at $\mu_0 H_p$=6.5 mT); (b) T_0 = 11 K and $\mu_0 H_p$ = 9.4 mT; (c) T_0 = 15 K and $\mu_0 H_p$ = 15.3 mT; (d) T_0 = 20 K and $\mu_0 H_a$ = 12 mT. The color bars indicate the local magnetic field component in mT. Panel (e) shows the average magnetic field in the central hole of the ring as a function of the applied field. (f) The threshold field $\mu_0 H_{th}$ for the onset of flux avalanches in superconducting rings of different sizes as a function of the inner radius R_i. The width $w = R_o - R_i$. The case of constant R_i and variable R_o is shown with blue squares and corresponds to the upper abscissa. Figure reproduced from [46].

radius is independent of the rim width [54] (see open star symbols in Fig.5(f)). However, H_{th} must depend on the sample size since the local field at the border of the ring is increased by a large geometric factor $\sim \mu_0 H\sqrt{R_o/d}$. Indeed, as shown in Fig.5(f), the threshold field for rings with a fixed rim width (the symbols connected by solid lines) and that for rings with a fixed R_i (the square symbols connected by a blue dotted line), both decrease with the radius R_o (upper axis) of the ring at different temperatures. This argument leads one to conclude that the threshold field should decrease with increasing R_o, as observed in Fig.5(f).

6 Domino effect in a double concentric ring configuration

Encouraged by the successful description of the experimental results based on the numerical modeling, Jiang et al.[46] explored experimentally and numerically the possibility of further protecting a ring by placing it inside another ring so as to

form a concentric double ring structure. Interestingly, it seems that this strategy does not really pay off since a flux jump in the outer ring triggers a flux jump in the inner ring, a phenomenon coined *domino effect* (see Fig.6). The authors of Ref.[46] suggest that during the process of magnetic perforation in the outer ring, the local current distribution decline near the preceding flux channel in the outer ring produces a ripple effect on the local magnetic field profile in the gap and at the edge of the inner ring. This effect ultimately leads to the domino effect of flux avalanches in the concentric rings. Namely, the domino effect of the thermomagnetic instability in such superconducting films with topological structures is not generated by the simple superpositions of flux behavior in the two rings, but depends on the competition between the divergence of the local field at the edge of the inner ring and the shielding by the neighboring ring. As expected, by decreasing the spacing between the concentric rings, the domino effect is reinforced.

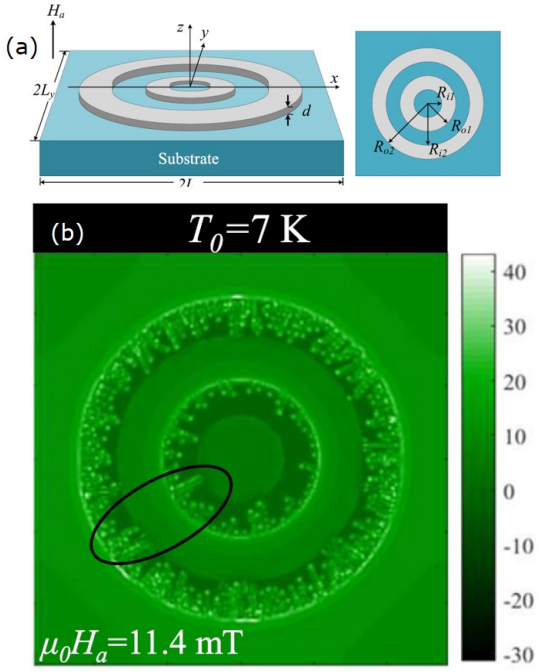

Fig. 6 Splitting a single ring into two concentric rings (a) can help to avoid avalanches in the inner ring when compared with the initial ring of the same outer diameter. (b) Simulated distribution of the out-of-plane magnetic field in two concentric superconducting rings after the formation of the first flux channel in the inner ring. The black ellipse indicates the loci of the magnetic perforation occurring almost simultaneously at the inner and outer rings (domino effect). Figure reproduced from [46].

Let us now compare the response of a single ring of outer diameter R_o and inner diameter R_i, with that corresponding to the same ring but split to form a double ring structure by removing material and introducing a gap. The inner ring will be labelled 1 and the outer ring 2 (as in Fig.6(a)), and the geometrical parameters will be $R_{i1} = R_i$, $R_{o2} = R_o$, $R_{o1} = R_o/2$, and $R_{i2} = 3R_o/4$. Fig. 7 shows the simulated distribution of magnetic field for the initial single ring (lower row) and for the split ring (upper row). For the double ring structure, when the applied field reaches 7.1 mT, a flux channel is formed in the outer superconducting ring, through which the

magnetic flux is injected into the outer hole and nucleates at multiple positions on the edge of the inner ring (see panel (a)). Remarkably, the flux channel in the concentric superconducting rings terminates at the outer hole, and does not extend to the central hole. With further increasing the applied field to 10 mT, there is still only one flux avalanche triggered in the concentric rings as shown in Fig. 7(b). However, at the same applied field of 10 mT, several flux avalanches occur in the single ring and form two flux channels (Fig. 7(d)). Surprisingly, the outer hole of the concentric rings shows a stabilization effect, somewhat reminiscence of the stop hole described in Ref.[56]. This result indicates that despite the domino effect, the two-concentric-rings structure cannot only reduce the scale and frequency of flux avalanches, but also effectively improves the thermomagnetic stability of the inner superconducting films, avoiding flux injection into the central hole of the system.

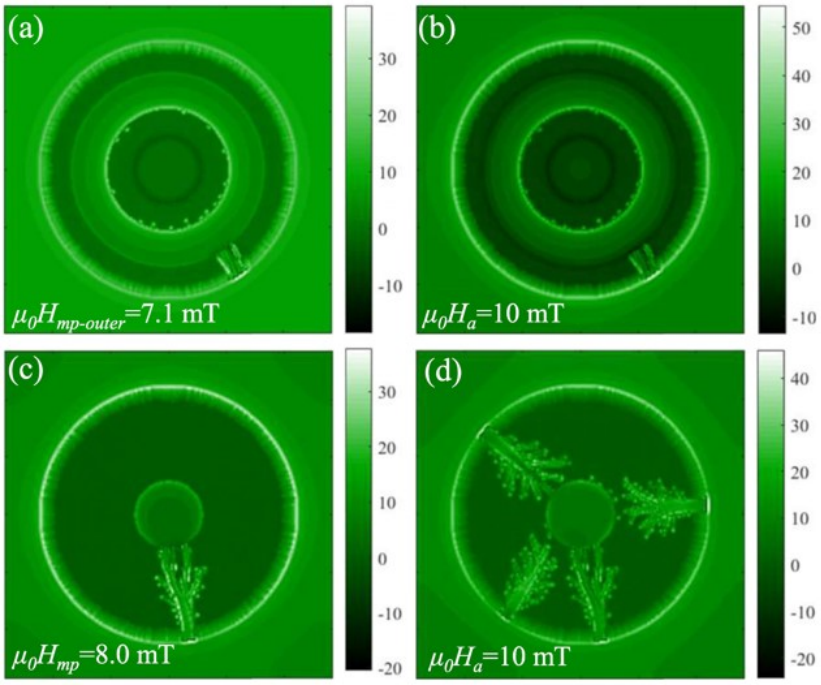

Fig. 7 Simulated distribution of magnetic field in two concentric superconducting rings [(a) and (b)], and in the single superconducting ring [(c) and (d)] for T = 10 K and field ramp rate 100 T/s. The smallest and largest diameters is the same for the two considered structures. The final applied field is indicated in the panels. Figure reproduced from [46].

The authors of Ref.[46] went further in their investigation and established a diagram indicating the different flux penetration regimes depending on the ratio between the outer radii of the concentric rings R_{o1}/R_{o2}, as shown in Fig. 8. In this figure, R_{o2} is fixed to 2.2 mm and therefore, as R_{o1} increases, the gap between the two rings closes up. The ordinate represents the threshold field for the thermomagnetic

instability *in the inner ring*. Note that the threshold field of the inner ring increases with R_{o1}. At small values of R_{o1}, the inner ring remains stable until the flux is injected into the outer hole through a perforated channel in the outer ring. In this regime, flux avalanches are triggered in the inner ring without the formation of flux channel connecting the outer hole and the central hole of the superconducting concentric rings. When R_{o1} increases above $\sim 0.52R_{o2}$, a crossing dendrite is formed in the inner ring following the magnetic perforation event in the outer ring. In other words, the first avalanche in the outer ring produces magnetic perforation which in turn triggers the first avalanche in the inner ring also giving rise to magnetic perforation. This is the so-called domino effect in which the flux is injected into the central hole of the superconductor, and develops when the gap between the rings is decreased below certain threshold value.

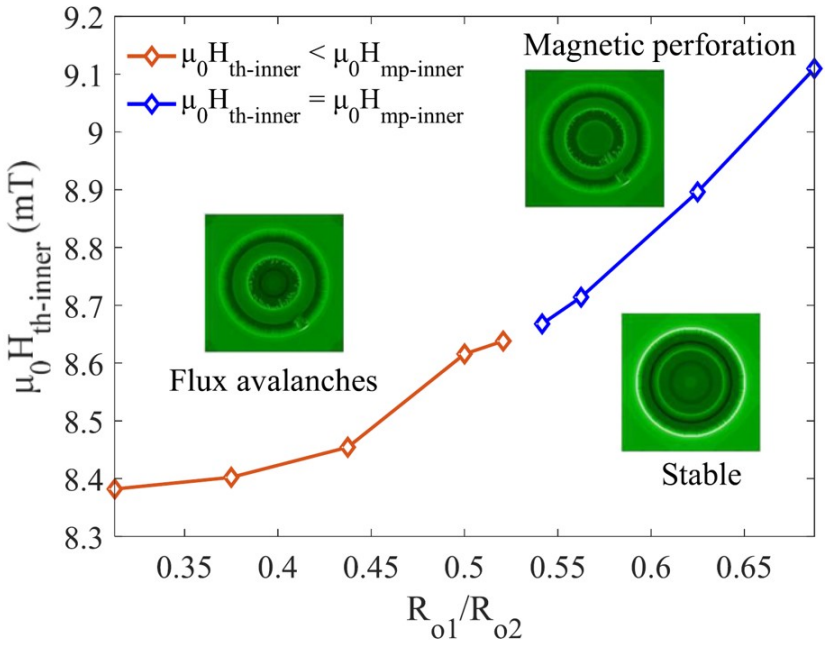

Fig. 8 Simulated threshold field $\mu_0 H_{th}$ for the onset of the avalanches in the inner ring $\mu_0 H_{th-inner}$ as a function of R_{o1}/R_{o2} with fixed R_{o2} = 2.2 mm for T = 11 K, field ramp rate of 100 T/s. The magnetic perforation takes place at an applied field $\mu_0 H_{mp}$. Figure reproduced from [46].

The study presented in this section may also have some implications for analyzing electric breakdown in multilayered dielectric heterostructures. In addition, it could be interesting to further explore the domino effect of thermomagnetic instability in several concentric rings (more than two rings).

7 Conclusion

In this chapter, we have succinctly discussed the process of magnetic flux filling in a macroscopic superconducting ring. Superconducting multiply-connected structures have found applications in a large diversity of domains, including storage rings, superconducting magnets, superconducting resonators, sensors, optical devices, magnetic traps, and many more for which the physics described in this chapter can be at play.

An elegant application of the physics of thermomagnetic instabilities in superconducting rings discussed in the previous sections appears in the response of superconducting resonators. Fig.9(a) schematically shows a quarter-wavelength superconducting resonator consisting in a coplanar waveguide with capacitively coupled resonators, all surrounded by a ground plane. This device is topologically similar to the structures indicated by the black arrows, which eventually evolve into ring structures. Therefore, it comes as no surprise that the different regimes appearing at $H < H_p$ (Meissner phase) and $H > H_p$ (magnetic perforation and subsequent dendritic avalanche triggering), have a direct impact on the quality factor of the resonator, as discussed in Ref.[57].

Furthermore, single-ring structures interrupted by a Josephson junction are the essential ingredient in rf superconducting interferometers [58, 77]. A similar configuration has been proposed by Savinov et al.[60] as a superconducting metamaterial where the array's motif consists of a superconducting loop surrounded by a split-ring resonator. In this system, an incident electromagnetic wave polarized along the split-ring resonator gap drives an oscillating current in the resonator, producing an oscillating magnetic field embraced by the split ring. For large enough excitations, the applied flux can induce transitions between the different quantum flux states of the inner ring, dynamically modifying the inductance and the resonant properties of the LC circuit (so-called *meta-molecule*).

Similarly, concentric superconducting ring structures might be relevant for low-frequency superconducting metamaterials [61, 62] and microstrip ring antennas[63]. In addition, diverse applications of superconducting rings can be identified, such as magnetic trapping of cold atoms [64] or as a condensed matter toy system to demonstrate the Zurek-Kibble scenario of early universe development [65]. In addition, it has been recently demonstrated theoretically the generation of supercurrent in superconducting rings under the influence of circularly polarized electromagnetic waves in the fluctuation regime above the critical temperature [66], the possibility to manipulate current-carrying states in a superconducting ring with circularly polarized radiation [67], and obtain chirality-controlled spontaneous currents in spin-orbit coupled superconducting rings [68]. Superconducting rings have also been proposed as a platform to store information which can be electrically controlled and accessed [69]. We have already evoked the qualities of superconducting cylinders to screen an axial magnetic field in ZFC conditions. In this context, it is particularly interesting the work of Brialmont et al. [70], which investigates the shielding properties of a stack of hundreds of ring-shaped YBCO coated conductors on ferromagnetic substrates. This system is intermediate between a single flat ring and a long cylinder. These authors demonstrate that at room temperature, the ferromagnetic material provides

a shielding factor > 1 for axial and transversal magnetic field directions. For temperatures below the superconducting transition of the YBCO, the superconducting layers contribute to the shielding of the axial component of the applied magnetic field, whereas the transverse component is mainly shielded by the ferromagnetic substrates of the tapes. The opposite behavior, i.e. to trap large amounts of magnetic flux and behave as permanent magnet, is also a very active line of technological research [71, 72, 73].

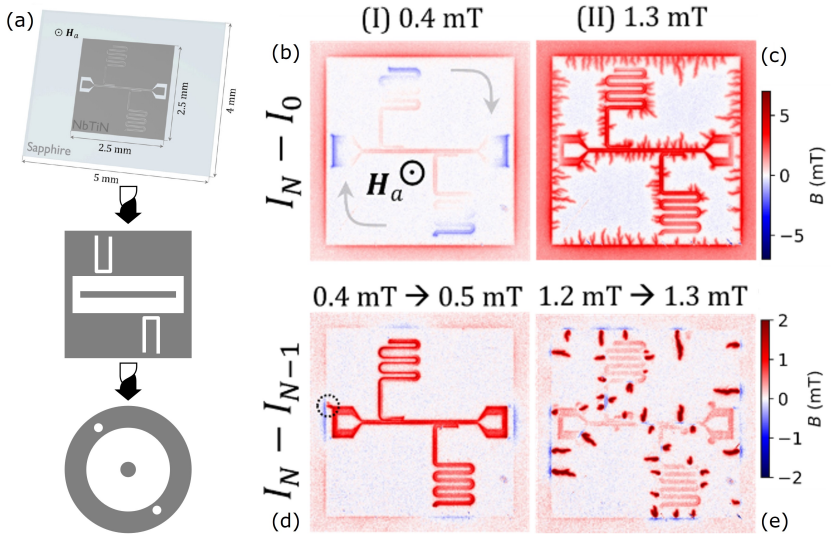

Fig. 9 (a) On-chip superconducting quarter-wavelength resonator and topologically similar structures. (b,c) Magneto-optical images of a NbTiN resonator as the one sketched in panel (a) for different applied fields: 0.4 mT (b) corresponding to the Meissner state and 1.3 mT (b) corresponding to magnetic flux avalanches regime. Panels (d,e) show the difference between consecutive images. Magnetic perforation indicated by a dotted circle in panel (d) leads to sudden injection of flux in the excitation line and the resonators (intense red color). New developing avalanches become apparent after differential imaging in panel (e). Figure reproduced from [57].

Concerning the perspectives of the research on superconducting rings, it would be interesting to dig further into 3D rings involving non-trivial topologies such as Möbius or eight-shape structures for which experimental investigations lag behind. Current nanofabrication techniques [74, 75, 76] are able to produce such intricate 3D architectures. Another research direction which deserves attention and for which much has already been done is the impact of surface defects (in the inner as well as outer rims) in addition to defects, imperfections, and pinning centres in the body of the ring. We have mainly focused on circular rings, under homogenous axial magnetic magnetic fields. A subject we have not touched upon in this Chapter is the response of rings to in-plane or tilted fields, particularly relevant for cloaking metasurfaces. We have also left out inhomogeneous fields, or loops with shapes

other than circular [77], for which current crowding and expanding may favour or disfavour privileged nucleation points of the normal phase. In all fairness, attempting to comprehensively address the physics of superconducting rings, including material, geometry, excitation frequency, temperature, and other parameters, represents a challenging task that goes beyond the scope of this Chapter. Actually, this Chapter does not intend to provide a comprehensive review of scientific contributions to the subject but rather to present a subjective view aimed at telling a story. Therefore, the literature and references discussed in this context should not be considered exhaustive. This story primarily concerns the unwanted and harmful appearance of flux avalanches in superconducting rings, which may be detrimental to the many foreseen applications involving this topology. The in-depth knowledge acquired on this particular problem should be instrumental in guiding us in the continuous quest for solutions and mitigation strategies to avoid thermomagnetic instabilities.

Acknowledgements The author is grateful to Maycon Motta, Benoît Vanderheyden, and Antonio Badía-Majós for the critical reading and valuable comments and remarks, which have improved the quality of this chapter's presentation.

References

1. W. A. Little. Decay of Persistent Currents in Small Superconductors. Phys. Rev. **156**, 396 (1967)
2. J. S. Langer, V. Ambegaokar. Intrinsic Resistive Transition in Narrow Suyerconducting Channels. Phys. Rev. **164**, 498 (1967)
3. J. E. Lukens, J. M. Goodkind. Flux Fluctuations and Critical Currents in a Superconducting Ring Near Tc. Phys. Rev. Lett. **20**, 1363 (1968)
4. L. D. Jackel, W. W. Webb, J. E. Lukens, S. S. Pei. Measurement of the probability distribution of thermally excited fluxoid quantum transitions in a superconducting ring closed by a Josephson junction. Phys. Rev. B **9**, 115 (1974)
5. X. Zhang, J. C. Price. Susceptibility of a mesoscopic superconducting ring. Phys. Rev. B **55**, 3128 (1997)
6. J. R. Kirtley, C. C. Tsuei, V. G. Kogan, J. R. Clem, H. Raffy, Z. Z. Li. Fluxoid dynamics in superconducting thin film rings. Phys. Rev. B **68**, 214505 (2003)
7. H. Polshyn, T. Naibert, R. Budakian. Imaging phase slip dynamics in micron-size superconducting rings. Phys. Rev. B **97**, 184501 (2018)
8. I. Petkovic, A. Lollo, L. I. Glazman, J. Harris. Deterministic phase slips in mesoscopic superconducting rings. Nat. Commun. **7**, 13551 (2016)
9. A. Bezryadin, C. N. Lau, M. Tinkham. Quantum suppression of superconductivity in ultrathin nanowires. Nature **404**, 971 (2000)
10. D. S. Golubev, A. D. Zaikin. Quantum tunneling of the order parameter in superconducting nanowires. Phys. Rev. B **64**, 014504 (2001)
11. M. Zgirski, K. Y. Arutyunov. Experimental limits of the observation of thermally activated phase-slip mechanism in superconducting nanowires. Phys. Rev. B **75**, 172509 (2007)
12. X. D. A. Baumans, et al. Thermal and quantum depletion of superconductivity in narrow junctions created by controlled electromigration. Nat. Commun. **7**, 10560 (2016)
13. W. A. Little, R. D. Parks. Observation of Quantum Periodicity in the Transition Temperature of a Superconducting Cylinder. Phys. Rev. Lett. **9**, 9 (1962); R. D. Parks, W. A. Little. Fluxoid Quantization in a Multiply-Connected Superconductor. Phys. Rev. **133**, A97 (1964)

14. R. P. Groff, R. D. Parks. Fluxoid Quantization and Field-Induced Depairing in a Hollow Superconducting Microcylinder. Phys. Rev. **176**, 567 (1968)
15. V. V. Moshchalkov, J. Fritzsche. Nanostructured Superconductors. World Scientific, Singapore (2011)
16. H. J. Fink, V. Grünfeld, A. López. Quantum-interference device without Josephson junctions. Phys. Rev. B **35**, 35 (1987)
17. V. V. Moshchalkov et al. Quantum interference in a mesoscopic superconducting loop. Nature **361**, 617 (1993)
18. O. J. Sharon, A. Shaulov, J. Berger, A. Sharoni, Y. Yeshurun. Current-induced SQUID behavior of superconducting Nb nano-rings. Scientific Reports **6**, 28320 (2016)
19. J. Berger, J. Rubinstein. Topology of the Order Parameter in the Little-Parks Experiment. Phys. Rev. Lett. **75**, 320 (1995)
20. E. M. Horane, J. I. Castro, G. C. Buscaglia, A. López. Transition between different quantum states in a mesoscopic system: The superconducting ring. Phys. Rev. B **53**, 9296 (1996)
21. K. K. Likharev. Superconducting weak links. Rev. Mod. Phys. **51**, 101 (1979)
22. A. G. Sivakov et al. Josephson Behavior of Phase-Slip Lines in Wide Superconducting Strips. Phys. Rev. Lett. **91**, 267001 (2003)
23. G. P. Papari, V. M. Fomin. Quantum interference in finite-size mesoscopic rings. Phys. Rev. B **105**, 144511 (2022)
24. E. H. Brandt. Susceptibility of superconductor disks and rings with and without flux creep. Phys. Rev. B **55**, 14513 (1997)
25. B.J. Baelus, F.M. Peeters, V.A. Schweigert. Saddle-point states and energy barriers for vortex entrance and exit in superconducting disks and rings. Phys. Rev. B **63**, 144517 (2001)
26. M. Lu-Dac, V. V. Kabanov. Multiple phase slips phenomena in mesoscopic superconducting rings. Phys. Rev. B **79**, 184521 (2009)
27. D.Y. Vodolazov, F.M. Peeters, S.V. Dubonovs, A.K. Geim. Multiple flux jumps and irreversible behavior of thin Al superconducting rings. Phys. Rev. B **67**, 054506 (2003)
28. A. Kanda, B.J. Baelus, D.Y. Vodolazov, J. Berger, R. Furugen, Y. Ootuka, F.M. Peeters. Evidence for a different type of vortex that mediates a continuous fluxoid-state transition in a mesoscopic superconducting ring. Phys. Rev. B **76**, 094519 (2007)
29. S. Pedersen, G. R. Kofod, J. C. Hollingbery, C. B. Sorensen, P. E. Lindelof. Dilation of the giant vortex state in a mesoscopic superconducting loop. Phys. Rev. B **64**, 104522 (2001)
30. I. Mowgood, G. Melkonyan, R. Dulal, S. Teknowijoyo, S. Chahid, A. Gulian. Violation of magnetic flux conservation by superconducting nanorings. Supercond. Sci. Technol. **35**, 045006 (2022)
31. F. Mila, C.A. Stafford, S. Capponi. Persistent currents in a Möbius ladder: A test of interchain coherence of interacting electrons. Phys. Rev. B **57**, 1457 (1998)
32. M. Hayashi, H. Ebisawa. Little-Parks Oscillation of Superconducting Möbius Strip. J. Phys. Soc. Jpn. **70**, 3495 (2001)
33. D. Y. Vodolazov, F. M. Peeters. Stable and metastable states in a mesoscopic superconducting "eight" loop in presence of an external magnetic field. Physica C **400**, 165 (2004)
34. Y. B. Kim, C. F. Hemptstead, A. R. Strnad. Magnetization and Critical Supercurrents. Phys. Rev. **129**, 528 (1963)
35. See Introduction to Superconductivity by Michael Tinkham, second edition, Dover Publications Inc. ISBN 0-486-43503-2 (2004) pp. 188-195, and references therein.
36. S. Denis, L. Dusoulier, M. Dirickx, Ph. Vanderbemden, R. Cloots, M. Ausloos, B. Vanderheyden. Magnetic shielding properties of high-temperature superconducting tubes subjected to axial fields. Supercond. Sci. Technol. **20**, 192 (2007)
37. M. Pannetier, F. C. Klaassen, R. J. Wijngaarden, M. Welling, K. Heeck, J. M. Huijbregrse, B. Dam, R. Griessen. Magneto-optical investigation of flux penetration in a superconducting ring. Phys. Rev. B **64**, 144505 (2001)
38. E. R. Nowak, O. W. Taylor, L. Liu, H. M. Jaeger, T. I. Selinder. Magnetic flux instabilities in superconducting niobium rings: Tuning the avalanche behavior. Phys. Rev. B **55**, 11702 (1997)

39. S. Blanco Alvarez, J. Brisbois, S. Melinte, R. B. G. Kramer, A. V. Silhanek. Statistics of thermomagnetic breakdown in Nb superconducting films. Scientific Reports **9**, 3659 (2019)
40. Å. A. F. Olsen, T. H. Johansen, D. Shantsev, E. Choi, H. Lee, H. J. Kim, S. Lee. Flux dendrites of opposite polarity in superconducting MgB2 rings observed with magneto-optical imaging. Phys. Rev. B **74**, 064506 (2006)
41. R. G. Mints, A. L. Rakhmanov. Critical state stability in type-II superconductors and superconducting-normal-metal composites. Rev. Mod. Phys. **53**, 551 (1981)
42. C. A. Durán, P. L. Gammel, R. E. Miller, D. J. Bishop. Observation of magnetic-field penetration via dendritic growth in superconducting niobium films. Phys. Rev. B **52**, 75 (1995)
43. J. I. Vestgården, D. V. Shantsev, Y. M. Galperin , T. H. Johansen. Lightning in superconductors. Scientific Reports **2**, 886 (2012)
44. National Academies of Sciences, Engineering, and Medicine (2008). Lightning-Warning Systems for Use by Airports. Washington, DC: The National Academies Press. https://doi.org/10.17226/14192.
45. Å. A. F. Olsen, T. H. Johansen, D. Shantsev, E. Choi, H. Lee, H. J. Kim, S. Lee. Avalanches injecting flux into the central hole of a superconducting MgB2 ring. Phys. Rev. B **76**, 024510 (2007)
46. Lu Jiang et al. Tunable domino effect of thermomagnetic instabilities in superconducting films with multiply-connected topological structures. New J. Phys. **24**, 083017 (2022)
47. Lu Jiang et al. Selective triggering of magnetic flux avalanches by an edge indentation. Phys. Rev. B **101**, 224505 (2020)
48. Liujiang Li et al. Tunable magnetic flux avalanches triggered by a focalized laser spot. Supercond. Sci. Technol. **35**, 085002 (2022)
49. A. I. Larkin, Yu.N. Ovchinnikov, Zh. Eksp. Teor. Fiz. **68**, 1915 (1975) [Nonlinear conductivity of superconductors in the mixed state. Sov. Phys. JETP **41**, 960 (1976)]
50. A. Andronov, I. Gordion, V. Kurin, I. Nefedov, I. Shereshevsky. Kinematic vortices and phase slip lines in the dynamics of the resistive state of narrow superconductive thin film channels. Physica C **213**, 193 (1993)
51. A. Silhanek et al. Formation of Stripelike Flux Patterns Obtained by Freezing Kinematic Vortices in a Superconducting Pb Film. Phys. Rev. Lett. **104**, 017001 (2010)
52. L. Embon, Y. Anahory, Ž.L. Jelić, E.O. Lachman, Y. Myasoedov, M.E. Huber, G.P. Mikitik, A.V. Silhanek, M.V. Milošević, A. Gurevich, E. Zeldov. Imaging of super-fast dynamics and flow instabilities of superconducting vortices. Nat. Commun. **8**, 85 (2017)
53. D. V. Denisov, D. V. Shantsev, Y. M. Galperin, Eun-Mi Choi, Hyun-Sook Lee, Sung-Ik Lee, A. V. Bobyl, P. E. Goa, A. A. F. Olsen, T. H. Johansen. Onset of dendritic flux avalanches in superconducting films. Phys. Rev. Lett. **97**, 077002 (2006)
54. J. Shvartzberg, A. Shaulov, Y. Yeshurun. Quasiperiodic magnetic flux avalanches in doubly connected superconductors. Phys. Rev. B **100**, 184506 (2019)
55. L. Burlachkov, N. Fuzailov. Staircase penetration of magnetic flux into a superconducting flat ring. Phys. Rev. B **107**, 224519 (2023)
56. F. Colauto, J. I. Vestgården, A. M. H. de Andrade, A. A. M. Oliveira, W. A. Ortiz, T. H. Johansen. Limiting thermomagnetic avalanches in superconducting films by stop-holes. Appl. Phys. Lett. **103**, 032604 (2013)
57. L. Nulens, N. Lejeune, J. Caeyers, S. Marinković, I. Cools, H. Dausy, S. Basov, B. Raes, M. J. Van Bael, A. Geresdi, A. V. Silhanek, J. Van de Vondel. Catastrophic magnetic flux avalanches in NbTiN superconducting resonators. Communications Physics **6**, 267 (2023)
58. A. H. Silver, J. E. Zimmerman. Quantum States and Transitions in Weakly Connected Superconducting Rings. Phys. Rev. **157**, 317 (1967)
59. L. Nulens, D. A. D. Chaves, O. J. Y. Harb, J. E. Scheerder, N. Lejeune, K. Brahim, B. Raes, A. V. Silhanek, M. J. Van Bael, J. Van de Vondel. Non-Invasive Readout of the Kinetic Inductance of Superconducting Nanostructures. Nanoletters (2024)
60. V. Savinov, A. Tsiatmas, A. R. Buckingham, V. A. Fedotov, P. A. J. de Groot, N. I. Zheludev. Flux Exclusion Superconducting Quantum Metamaterial: Towards Quantum-level Switching. Scientific Reports **2**, 450 (2012)

61. J. Prat-Camps, A. Sanchez, C. Navau. Superconductor–ferromagnetic metamaterials for magnetic cloaking and concentration. Supercond. Sci. Technol. **26**, 074001 (2013); J. Prat-Camps, C. Navau, A. Sanchez. Experimental realization of magnetic energy concentration and transmission at a distance by metamaterials. Appl. Phys. Lett. **105**, 234101 (2014)
62. N. Lejeune, E. Fourneau, A. Barrera, O. Morris, O. Leonard, J. A. Arregi, et al. Dimensional crossover of microscopic magnetic metasurfaces for magnetic field amplification. APL Mater. **12**, 071126 (2024)
63. F. Schettino. Analytically Regularized Evaluation of the Coupling of Planar Concentric Conducting Rings. Appl. Sci. **13**, 218 (2023)
64. P. Weiss, M. Knufinke, S. Bernon, D. Bothner, L. Sárkány, C. Zimmermann, R. Kleiner, D. Koelle, J. Fortágh, H. Hattermann. Sensitivity of Ultracold Atoms to Quantized Flux in a Superconducting Ring. Phys. Rev. Lett. **114**, 113003 (2015)
65. R. Monaco, J. Mygind, R. J. Rivers, V. P. Koshelets. Spontaneous fluxoid formation in superconducting loops. Phys. Rev. B **80**, 180501 (2009)
66. V. D. Plastovets, A. I. Buzdin. Fluctuation-mediated inverse Faraday effect in superconducting rings. Physics letters A **481**, 129001 (2023)
67. M. D. Croitoru, S. Mironov, B. Lounis, A. I. Buzdin. Toward the Light-Operated Superconducting Devices: Circularly Polarized Radiation Manipulates the Current-Carrying States in Superconducting Rings. Advanced quantum technologies **5**, 2200054 (2022)
68. J. W. A. Robinson, A. V. Samokhvalov, A. V. Samokhvalov, A. I. Buzdin. Chirality-controlled spontaneous currents in spin-orbit coupled superconducting rings. Phys. Rev. B **99**, 180501 (2019)
69. A. Kenawy, W. Magnus, M. V. Milošević, B. Sorée. Voltage-controlled superconducting magnetic memory. AIP Advances **9**, 125223 (2019)
70. S. Brialmont, J. Dular, L. Wéra, J-F. Fagnard, B. Vanderheyden, Ch. Geuzaine, S. Hahn, A. Patel, Ph. Vanderbemden. Magnetic shielding up to 0.67 T at 77 K using a stack of high temperature superconducting tape annuli of 26 mm bore. Supercond. Sci. Technol. **36**, 054004 (2023)
71. Jinhong Shi, Bing Wang, Boyang Shen, Jie Sheng. Numerical Study on Ring-shape Superconducting Trapped Field Magnet Based on Circuit Model. IEEE Transactions on Applied Superconductivity **31**, 4901605 (2021)
72. S. B. Kim, T. Kimoto, S. Hahn, Y. Iwasa, J. Voccio, M. Tomita. Study on optimization of YBCO thin film stack for compact NMR magnets. Physica C **484**, 295 (2013)
73. X. Yuan, Y. Wang, Y. Hou, C. Kan, C. Cai, M. Sun. Conceptual Design of a Bitter-Like Superconducting Magnet Stacked by REBCO Annular Plates and Magnetized by Flux Pump. IEEE Trans. Appl. Supercond. **28**, 4603005 (2018)
74. J. M. De Teresa, A. Fernández-Pacheco, R. Córdoba, L. Serrano-Ramón, et al. Review of magnetic nanostructures grown by focused electron beam induced deposition (FEBID). Journal of Physics D: Applied Physics **49**, 243003 (2016)
75. D. Makarov, O. M. Volkov, A. Kákay, O. V. Pylypovskyi, B. Budinská, et al.New Dimension in Magnetism and Superconductivity: 3D and Curvilinear Nanoarchitectures. Advanced Materials **34**, 2101758 (2021)
76. M. Huth, F. Porrati, O. V. Dobrovolskiy. Focused electron beam induced deposition meets materials science. Microelectronic Engineering **185**, 9 (2018)
77. L. Nulens, D. A. D. Chaves, O. J. Y. Harb, J. E. Scheerder, N. Lejeune, K. Brahim, B. Raes, A. V. Silhanek, M. J. Van Bael, J. Van de Vondel, Noninvasive Readout of the Kinetic Inductance of Superconducting Nanostructures. Nano Lett. **24**, 11149 (2024)